Amyotrophic lateral sclerosis models derived from human embryonic stem cells with different superoxide dismutase 1 mutations exhibit differential drug responses.

AUTHOR(S):

Isobe, Takehisa; Tooi, Norie; Nakatsuji, Norio; Aiba, Kazuhiro

CITATION:

Isobe, Takehisa ...[et al]. Amyotrophic lateral sclerosis models derived from human embryonic stem cells with different superoxide dismutase 1 mutations exhibit differential drug responses.. Stem cell research 2015, 15(3): 459-468

ISSUE DATE:

2015-09-24

URL:

http://hdl.handle.net/2433/202584

Stem Cell Research 15 (2015) 459–468

Contents lists available at ScienceDirect

Stem Cell Research

journal homepage: www.elsevier.com/locate/scr

Amyotrophic lateral sclerosis models derived from human embryonic stem cells with different superoxide dismutase 1 mutations exhibit differential drug responses

Takehisa Isobe [a,b], Norie Tooi [a], Norio Nakatsuji [a,c], Kazuhiro Aiba [a,*]

[a] Institute for Integrated Cell-Material Sciences (WPI-iCeMS), Kyoto University, Kyoto 606-8501, Japan
[b] Graduate School of Medicine, Kyoto University, Kyoto 606-8501, Japan
[c] Institute for Frontier Medical Sciences, Kyoto University, Kyoto 606-8507, Japan

ARTICLE INFO

Article history:
Received 15 September 2015
Accepted 15 September 2015
Available online 24 September 2015

Keywords:
Amyotrophic lateral sclerosis
SOD1
Human embryonic stem cell
Motor neuron
Drug response

ABSTRACT

Amyotrophic lateral sclerosis (ALS) is a neurodegenerative motor neuron (MN) disease. The gene encoding superoxide dismutase 1 (SOD1) is a causative element of familial ALS. Animal ALS models involving SOD1 gene mutations are widely used to study the underlying mechanisms of disease and facilitate drug discovery. Unfortunately, most drug candidates have failed in clinical trials, potentially due to species differences among rodents and humans. It is unclear, however, whether there are different responses to drugs among the causative genes of ALS or their associated mutations. In this study, to evaluate different SOD1 mutations, we generated SOD1-ALS models derived from human embryonic stem cells with identical genetic backgrounds, except for the overexpression of mutant variants of SOD1. The overexpression of mutant SOD1 did not affect pluripotency or MN differentiation. However, mutation-dependent reductions in neurite length were observed in MNs. Moreover, experiments investigating the effects of specific compounds revealed that each ALS model displayed different responses with respect to MN neurite length. These results suggest that SOD1 mutations could be classified based the response of MNs to drug treatment. This classification could be useful for the development of mutant-specific strategies for drug discovery and clinical trials.

1. Introduction

Amyotrophic lateral sclerosis (ALS) is a fatal neurodegenerative disease characterized by death of both upper and lower motor neurons (MNs) (Beckman et al., 2001). About 90% of ALS cases are sporadic. The remaining 10% of cases are classified as familial ALS (FALS), which is characterized by mutations in genes including superoxide dismutase 1 (SOD1), transactive response DNA-binding protein 43 kDa (TARDBP, TDP-43), fused in sarcoma (FUS) and chromosome 9 open reading frame 72 (C9ORF72) (Rosen et al., 1993) (Neumann et al., 2006) (Vance et al., 2009) (Renton et al., 2011). Approximately 20% of FALS cases are caused by mutations in the SOD1 gene, and over a hundred SOD1 mutations have been reported to date (Renton et al., 2014). The average age at onset of SOD1-related ALS (SOD1-ALS) is 55 years; the primary hallmark of both SOD1-ALS and other forms of the disease is death of MNs leading to muscle weakness (Lyall et al., 2001) (Millecamps et al., 2010) (Bruijn et al., 2004). Riluzole is the drug approved for the treatment of ALS, and is effective in the extension of the patient's lifetime for a relatively limited duration. Hence, there is a great demand for more efficacious drugs. Although many candidate drugs for ALS have been discovered using animal models, almost all of these drugs have failed clinical trials, potentially because of species differences in drug responses among rodents and human beings (Glicksman, 2011) (Limpert et al., 2013).

Human pluripotent stem cell (hPSCs)-based disease models are promising tools to overcome the problems associated with species differences. Recently, studies reported cellular ALS models that used hPSCs including human embryonic stem cells (hESCs) and induced pluripotent stem cell (iPSCs). Using these models, MN death was observed, indicating an ALS phenotype (Wada et al., 2012) (Bilican et al., 2012). Additionally, new drug candidates, kenpaullone and anacardic acid were discovered (Egawa et al., 2012; Yang et al., 2013). However, because these models do not generally have an identical genetic

Abbreviations: ALS, amyotrophic lateral sclerosis; cAMP, cyclic adenosine monophosphate; dbcAMP, dibutyryl-cAMP; DMSO, dimethyl sulfoxide; hESCs, human embryonic stem cells; hPSCs, human pluripotent stem cell; HPRT1, hypoxanthine phosphoribosyltransferase 1; iPSCs, induced pluripotent stem cell; MN, motor neuron; MRB, mutants and metal-binding region; ROCK, Rho-associated protein kinase; RT-PCR, reverse transcription polymerase chain reaction; SOD1, superoxide dismutase 1; SOD1-hESCs, SOD1-overexpressing hESCs; WT, wild-type.

* Corresponding author at: Institute for Integrated Cell-Material Sciences (WPI-iCeMS), Kyoto University Yoshida-Ushinomiyacho, Sakyo-ku, Kyoto 606-8501, Japan.
E-mail address: kaiba@icems.kyoto-u.ac.jp (K. Aiba).

http://dx.doi.org/10.1016/j.scr.2015.09.006
1873-5061/

background, it is difficult to accurately compare results among the various mutations in ALS-related genes.

Here, to investigate the specific differences among SOD1 mutations, we generated hESC-derived models of SOD1-ALS with identical genetic backgrounds, except for those resulting in the overexpression of SOD1 variants. We found no differences in pluripotency or the ability to differentiate into MNs among any of the SOD1-overexpressing hESCs (SOD1-hESCs). Our cell model also demonstrated mutant-specific phenotypes including mutant-dependent reduction in MN neurite length. Additionally, using several compounds, we found that each ALS model showed different responses to these compounds.

2. Materials and methods

2.1. Establishment of SOD1-overexpressing hESC lines

HESCs were cultured on mitomycin-C-treated mouse embryonic fibroblasts in primate ES medium (ReproCELL, Japan), supplemented with 5 ng/mL fibroblast growth factor 2 (Wako Chemicals, Japan), as previously described (Suemori et al., 2006). To generate WT or mutant SOD1 overexpressing hESCs, the site-specific gene integration method, which we developed previously (Sakurai et al., 2010), was applied. Both the SOD1 and Cre recombinase expression vectors were introduced into the parental hESCs derived from the hESC line KhES-1 (Suemori et al., 2006). SOD1 cDNAs in the expression vector were integrated into the HPRT1 locus on the genome of the parental hESCs. Hygromycin-resistant clones, which showed normal cell growth, were isolated and used as SOD1-overexpressing hESCs (SOD1-hESCs). Karyotype analysis was carried out by Nihon Gene Research Laboratories, Inc. The hESC lines were used in accordance with the Guidelines for Derivation and Utilization of Human Embryonic Stem Cells proposed by the Ministry of Education, Culture, Sports, Science, and Technology (MEXT) of Japan.

2.2. Immunocytochemistry

Cells were fixed in both 4% paraformaldehyde (Nacalai Tesque, Japan) and 4% sucrose (Wako), and permeabilized using 0.2% Triton X-100 (Nacalai Tesque, Japan). After blocking with 1.5% bovine serum albumin at room temperature, cells were incubated with a primary antibody overnight, followed by a secondary antibody for 1 h at 4 °C. The primary antibodies used in this study were mouse anti-OCT3/4 monoclonal antibody (mAb) (Santa Cruz Biotechnology), rabbit anti-NANOG polyclonal antibody (pAb; Cell Signaling Technology), mouse anti-SSEA4 mAb (Millipore), mouse anti-TRA-1–60 mAb (Millipore), rabbit anti-nestin pAb (Millipore), mouse anti-OLIG2 mAb (Millipore), mouse anti-ISL-1/2 mAb (Developmental Studies Hybridoma Bank), mouse anti-MNR2 mAb (HB9, Developmental Studies Hybridoma Bank), mouse anti-TUJ1 mAb (Sigma-Aldrich), and rabbit anti-MAP2 pAb (Millipore). Secondary antibodies used in this study were goat anti-mouse immunoglobulin-G pAb conjugated with Alexa Fluor 488 or 546 (Molecular Probes), and goat anti-rabbit immunoglobulin-G pAb conjugated with Alexa Fluor 488 or 546 (Molecular Probes). Cells were counterstained with 4′,6-diamidino-2-phenylindole (DAPI) for visualization of all nuclei after the treatment of secondary antibody. Image acquisition was performed using an inverted Olympus IX71 epi-fluorescence microscope with an Olympus DP73 CCD camera (Olympus). Images were randomly captured from more than six or ten fields per single experiment to calculate MN differentiation rates or for measuring MN morphologies, respectively. The neurite length and soma sizes of neurons were measured by CellSens Dimension software (Olympus).

2.3. Western blot analysis

Confluent hESCs were dissolved with cold RIPA buffer (Sigma) supplemented with halt protease and phosphatase inhibitor cocktail (Thermo Scientific) and mixed using a vortex mixer. Lysates were centrifuged at 12,000 rpm for 20 min at 4 °C and the supernatants were used as protein samples. Protein concentrations were measured using the Pierce BCA Protein Assay Kit (Thermo Scientific). Protein samples were diluted with 4× Laemmli Sample Buffer (Bio Rad) and 2-mercaptoethanol (Wako) and then boiled at 95 °C for 5 min. Samples were electrophoresed through 4–20% precast gel (Cosmo Bio Co., Japan) with Tris/Glycine/SDS Buffer (Bio Rad), and then transferred to polyvinylidene difluoride membranes (Bio Rad) with Tris/Glycine Buffer (Bio Rad). After treatment with Blocking One solution (Nacalai Tesque), membranes were incubated with a primary antibody overnight at 4 °C and then incubated with a secondary antibody for 1 h at room temperature. To visualize proteins bonding with antibodies, the Novex ECL HRP Chemiluminescent Substrate Reagent Kit (Invitrogen) and the luminescent image analyzer LAS3000 (Fujifilm) were used. Quantification of the band intensity was performed by Multi Gauge software (Fujifilm). The primary antibodies used in this study were rabbit anti-superoxide dismutase1 pAb (Abcam), rabbit anti-superoxide dismutase pAb (Stressgen), and mouse anti-β-actin mAb (Abcam). The secondary antibodies used were anti-mouse IgG HRP-linked antibody (Cell Signaling), goat anti-rabbit IgG HRP-linked antibody (Santa Cruz).

2.4. Motor neuron differentiation

Two MN differentiation methods were carried out in this study (Supplementary Fig. S2). The first was our previous method with a slight modification (Wada et al., 2012; Wada et al., 2009) (Supplementary Fig. S2A). Briefly, a bone morphogenetic protein inhibitor, LDN193189 (200 nM; Cellagen Technology), was used as a neural inducer (stage P1, shown in Supplementary Fig. S2A). In stage P2, cells were treated with 200 nM LDN193189 and 100 nM all-trans retinoic acid (ATRA; Sigma-Aldrich) in N2B27 neural differentiation medium (NDM). Neural rosettes in the P2 cells were re-plated on poly-L-lysine/laminin/fibronectin (PLL/LM/FN)-coated culture dishes and cultured in NDM supplemented with 2.5 μM ATRA, 1 μM purmorphamine (Cayman Chemical), and 2.5 μM CHIR99021 (R&D). After 2 days, the medium was changed to NDM supplemented with 1 μM ATRA, 1 μM purmorphamine (Tocris Bioscience), and 1 μM CHIR99021, and cells were cultured for 5 days. Then, the cells were cultured in NDM containing 10 ng/mL brain-derived neurotrophic factor (BDNF; PeproTech), 10 ng/mL glial cell-derived neurotrophic factor (GDNF; PeproTech), and 10 ng/mL neurotrophin-3 (NT-3; PeproTech) for another 2 weeks.

The second differentiation method was established in this study (Supplementary Fig. S2B). For neural induction, dissociated ES colonies were grown on PLL/LM-coated culture dishes in NDM supplemented with 200 nM LDN193189 and 1 μM SB431542 for 8 days (stage P1, shown in Supplementary Fig. S2B). The medium was changed every other day. Primary colonies were split into small groups of cells using 200 U/mL collagenase with 1 mM $CaCl_2$, plated on new PLL/LM-coated culture dishes, and cultured in NDM supplemented with 200 nM LDN193189 (stage P2, shown in Supplementary Fig. S2B) for 8 days. Then, cells were re-plated and cultured in NDM alone for 8 days. Neural rosettes formed during the P3 stage. Neural rosettes were dissociated using Accutase (Innovative Cell Technologies, Inc) and plated onto gelatin-coated culture dishes for 45–60 min at 37 °C to remove non-neural cells. Unattached cells were then cultured on PLL/LM/FN-coated culture dishes in NDM supplemented with 0.5 μM ATRA, 0.5 μM purmorphamine, 0.5 μM CHIR99021, 10 ng/mL BDNF, 10 ng/mL GDNF, and 10 ng/mL NT-3 for 7 days. For long-term culture in the P4 stage, cells were treated 1 μM Cytarabine (AraC), and the medium was changed every 7 days.

2.5. Chemicals

Kenpaullone and riluzole were purchased from Cayman Chemical. Y27632 and dbcAMP were purchased from Wako Chemicals. TRO19622

were purchased from Sigma. MCI-186 was purchased from Focus Biomolecules. The treatment with these chemicals was performed from d3 to d7 (over a 4-day period) on cells in stage P4 (Supplementary Fig. S2B). The chemical concentrations used in this study in Fig. 5 were same as reported in previous studies except MCI-186 (Rojas et al., 2014) (Bryan et al., 2006) (Gunther et al., 2014) (Yang et al., 2013) (Bordet et al., 2007).

2.6. RNA isolation and PCR analysis

Total RNA was extracted using an RNeasy Kit (Qiagen), and cDNA was synthesized using ReverTra Ace qPCR RT Master Mix (Toyobo, Japan). PCR was performed using KOD FX (Toyobo, Japan) or TaKaRa Ex Taq (TaKaRa, Japan). The primers used in this study are shown in Supplementary Table S2.

2.7. SOD enzyme assay

The enzymatic activity of SOD was measured using an SOD Assay kit-WST (Dojindo Molecular Technologies Inc., Japan) according to the manufacturer's protocol. In brief, hESCs were centrifuged at 12,000 rpm for 30 min at 4 °C. Pellets were dissociated with phosphate buffered saline, and freezing and thawing steps were repeated three times. After centrifugation, the supernatants were used as samples in this experiment. The absorbance of the samples was measured using an ARVO MX 1420 Multilabel Counter microplate reader (Perkin Elmer).

2.8. Statistical analysis

Each experiment was independently performed three or more times ($n \geq 3$). Statistical differences were analyzed by the non-parametric Kruskal—Wallis test followed by the Dunn's multiple comparison test or the Steel's test for three or more group comparisons, and the Mann–Whitney U test for pairwise comparisons. Differences were considered significant at $P < 0.05$.

3. Results

3.1. No variations among SOD1-overexpressing hESC clones

Wild-type (WT) or mutant SOD1-hESCs were established by using the site-specific gene integration method (Sakurai et al., 2010). In our gene-integration system, the acquisition of drug resistance indicates that the integration of the correct gene has occurred at the hypoxanthine phosphoribosyltransferase 1 (HPRT1) locus. Using either two or three drug-resistant clones with the same mutations, we examined whether there were any variations in SOD1 gene or protein expression among the SOD1-hESC clones. Analysis of semi-quantitative reverse transcription polymerase chain reaction (RT-PCR) showed that all SOD1-hESCs expressed exogenous SOD1 with no changes in endogenous expression levels (Fig. 1A). These data suggest that the ectopic expression of exogenous SOD1 did not influence the endogenous expression of the gene. Next, the SOD1 protein levels were measured by Western blot. The expression levels of WT-, A4V- and G93A-SOD1 protein variants in SOD1-hESCs were approximately 2.0-fold higher than that in the parent cells (Fig. 1B). The expression levels of G85R-SOD1 (comprising the total amount of 2 bands) were almost 1.5-fold higher than that in parent cells (Fig. 1B). Statistical analysis indicated no significant differences in SOD1 protein levels among clones with the same mutations, as expected. Immunostaining showed that the fluorescence intensity of SOD1 in mutant SOD1-hESCs was higher than that in parent cells, showing that SOD1 was overexpressed in hESCs, but it did not form aggregates (Supplementary Fig. S1). The enzymatic activities of SOD in WT-, A4V-, and G93A-SOD1-hESCs were approximately 2.5-fold, 1.5-fold, and 2.5-fold higher, respectively, than that of the parent (Fig. 1C). However, there were no statistical significant differences in the SOD activities among clones with the same mutations. A4V-SOD1 is less stable than WT-SOD1 (Borchelt et al., 1994). Thus, the observed fold-increase of enzymatic activity for this variant is expected to be lower than that of WT and G93A-SOD1. G85R-SOD1 lacks enzymatic activity due to an ion binding deficiency (Hayward et al., 2002). As expected, no SOD activity above the levels in parent cells was detected in G85R-SOD1-hESCs (Fig. 1C). The combined data show that there were no significant variations in SOD activity or SOD1 protein expression levels among any of the mutant-SOD1 clones. A single clone for each mutant SOD1-hESC line was therefore chosen for further experiments.

3.2. SOD1 overexpression did not influence the undifferentiated state of hESCs

To assess the pluripotency of SOD1-hESCs, we examined the expression of specific markers of pluripotency by immunocytochemistry and RT-PCR. Immunocytochemistry data indicated that all SOD1-hESC

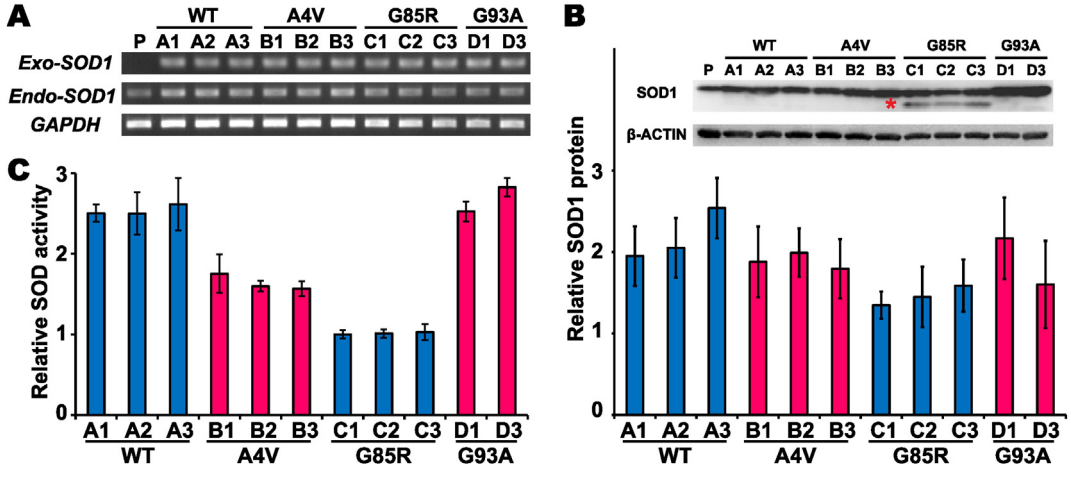

Fig. 1. No variations in expression among SOD1-hESC clones. (A) RT-PCR analysis of exogenous and endogenous SOD1 gene expression in undifferentiated hESCs. GAPDH was used as a loading control. Exo: exogenous-, Endo: endogenous-SOD1. (B) Quantitative analysis of SOD1 protein in undifferentiated hESCs using data obtained by Western blot (WB). The inset shows representative SOD1 protein WB data in undifferentiated hESCs. The asterisk indicates that G85R-SOD1 that has different mobility from that of WT-SOD1 in the WB assay (Wang et al., 2009). β-ACTIN was used as a loading control. The expression level of SOD1 in the parent hESCs was defined as 1. Values represent means ± standard deviation (SD) ($n = 5$). (C) Relative enzymatic activity of SOD in undifferentiated hESCs. The activity level of SOD in the parent hESCs was defined as 1. Values represent means ± SD ($n = 4$). P, parent hESC; WT, wild type; A, WT-SOD1; B, A4V-SOD1; C, G85R-SOD1; D, G93A-SOD1. Numbers indicate clone identification number.

lines expressed pluripotency markers including OCT3/4, NANOG, SSEA4, and TRA-1-60 (Fig. 2A). RT-PCR analysis showed that the pluripotency markers NANOG and OCT3/4 were expressed in all cell lines (Fig. 2B). These results show that overexpression of WT and mutant SOD1 did not affect the pluripotency of SOD1-hESCs.

SOD1-hESCs were similar to the parent hESCs in measures of cell proliferation (Fig. 2C). All SOD1-hESCs also maintained a normal female karyotype (46XX) with no numerical abnormalities (Fig. 2D). These data indicate that overexpression of WT or mutant SOD1 did not affect cell proliferation or chromosome stability.

3.3. SOD1 overexpression did not affect neural differentiation in hESCs

To determine the effects of mutant SOD1 on neural differentiation, we generated spinal motor neurons (MNs) from hESCs as described previously (Wada et al., 2009) (Supplementary Fig. S2A). We first compared the efficiency of MN differentiation among all SOD1-hESCs and the parent cells (Fig. 3A). On day 10 in P2 (P2-d10), differentiated cells contained approximately 15% OLIG2-positive MN progenitors in all SOD1-hESCs. The rates of differentiation were not statistically different among the parent cells and those expressing SOD1 mutants (Fig. 3B). The proportion of OLIG2-positive MN progenitors increased to as high as 70% on P3-d7 and decreased to 50% on P3-d14 (Fig. 3C). During the P3 stage, there were no differences in differentiation efficiency among cells. On P3-d21, all SOD1-hESCs expressed MN markers including ISL1, HB9 and choline acetyltransferase (Fig. 3G). The relative proportions of ISL1-positive or HB9-positive MNs were approximately 15% and 10%, respectively (Fig. 3D). To detect the exogenous SOD1 gene expression, RT-PCR was performed. Exogenous SOD1 and other neuron-specific markers were detected at P2-d10, P3-d14 and P3-d21 (Fig. 3E, F and G). These data suggest that both WT and mutant SOD1-hESCs had similar neural differentiation efficiencies compared to that of the parent cells, further indicating that overexpression of SOD1 did not influence neuronal differentiation.

3.4. Mutant SOD1 induced morphological changes in MNs overexpressing SOD1

Next, we assessed the influences of mutant SOD1 on MN morphologies using a separate differentiation method developed in this study (shown in Supplementary Fig. S2B). We found no significant differences among cell lines with respect to the ratio in percentages of ISL1-positive MNs to MAP2-positive neurons on d7, d14 and d21 in P4 (Fig. 4A). RT-PCR analysis indicated that exogenous SOD1s were expressed in WT and mutant cell lines on P4-d14 (Fig. 4B). Next, we examined three morphological parameters, viz., soma size, the number of branches and the longest neurite length (Supplementary Fig. S3). The expansions of soma sizes among the cells were observed over time; no changes were detected in the MNs derived from parental cell lines between d14 and d21 in P4 (Fig. 4C). The number of branches in ISL1, MAP2 double-positive MNs was not different among any SOD1-hESCs or the parent cells (Fig. 4D). Although there were no differences in soma size or branch numbers, we found that different SOD1 mutations showed different phenotypes with respect to the longest neurite observed in SOD1-hESC-derived neurons. The longest neurite of ISL1, MAP2 double-positive MNs was shorter in A4V- and G93A-MNs compared to that in the parent-MNs, but not in WT- and G85R-MNs (Fig. 4E). On the other hand, the longest neurite of ISL1-negative, MAP2-positive non-MNs got longer in G85R-non-MNs compared to that in the parent cells (Fig. 4F). These data indicate that the expression of A4V- and G93A-SOD1 only affected MNs, whereas that of G85R-SOD1 specifically affected non-MNs in our cellular models. The neurite length of G85R-MNs was not altered, but the expression of G85R-SOD1 might lead to other cellular phenotypes that we did not examine in this study.

3.5. SOD1-MNs with different mutations displayed differences in responses to compounds

To examine whether there are the specific differences among mutant SOD1-MNs, we treated our ALS model cells with six compounds,

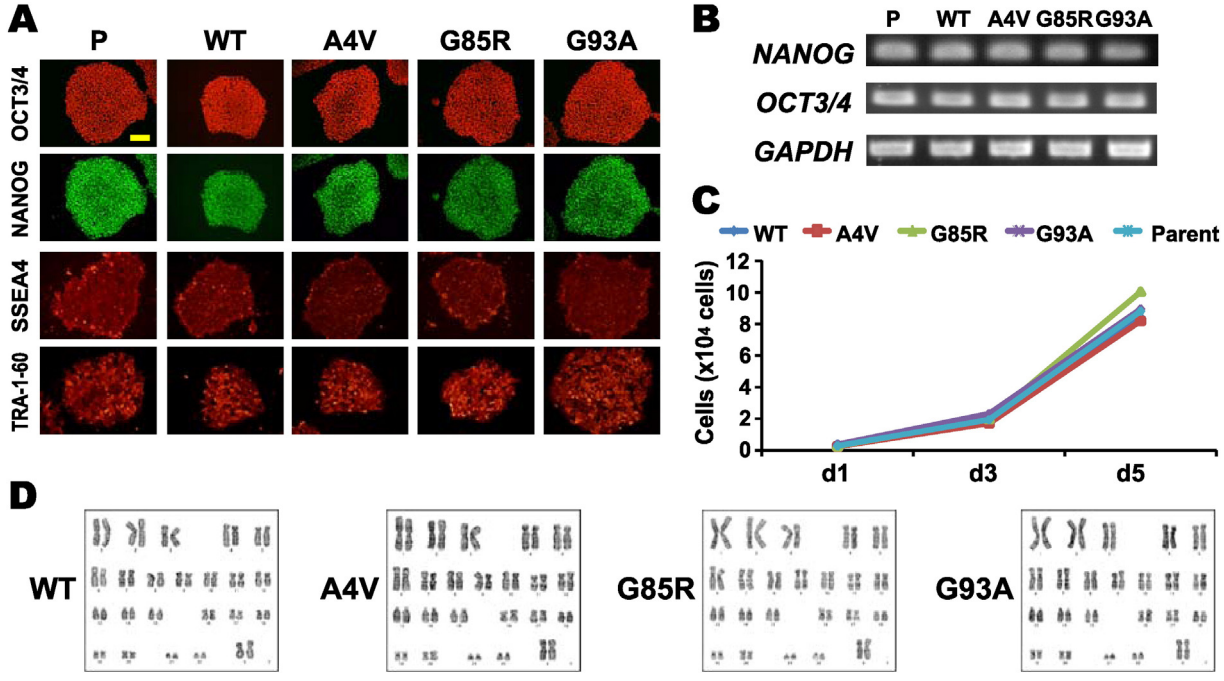

Fig. 2. Characterization of undifferentiated SOD1-hESCs. (A) Immunocytochemistry of the following pluripotency markers in undifferentiated SOD1-hESCs: OCT3/4, NANOG, SSEA4, and TRA-1–60. Scale bar, 100 μm. (B) RT-PCR analysis of pluripotency markers in undifferentiated hESCs. GAPDH was used as a loading control. (C) Cell proliferation of undifferentiated SOD1-hESCs (n = 3). Fifty thousand cells were plated on a Matrigel-coated well of 96-well plates on d0. (D) Karyotype analysis in undifferentiated SOD1-hESCs.

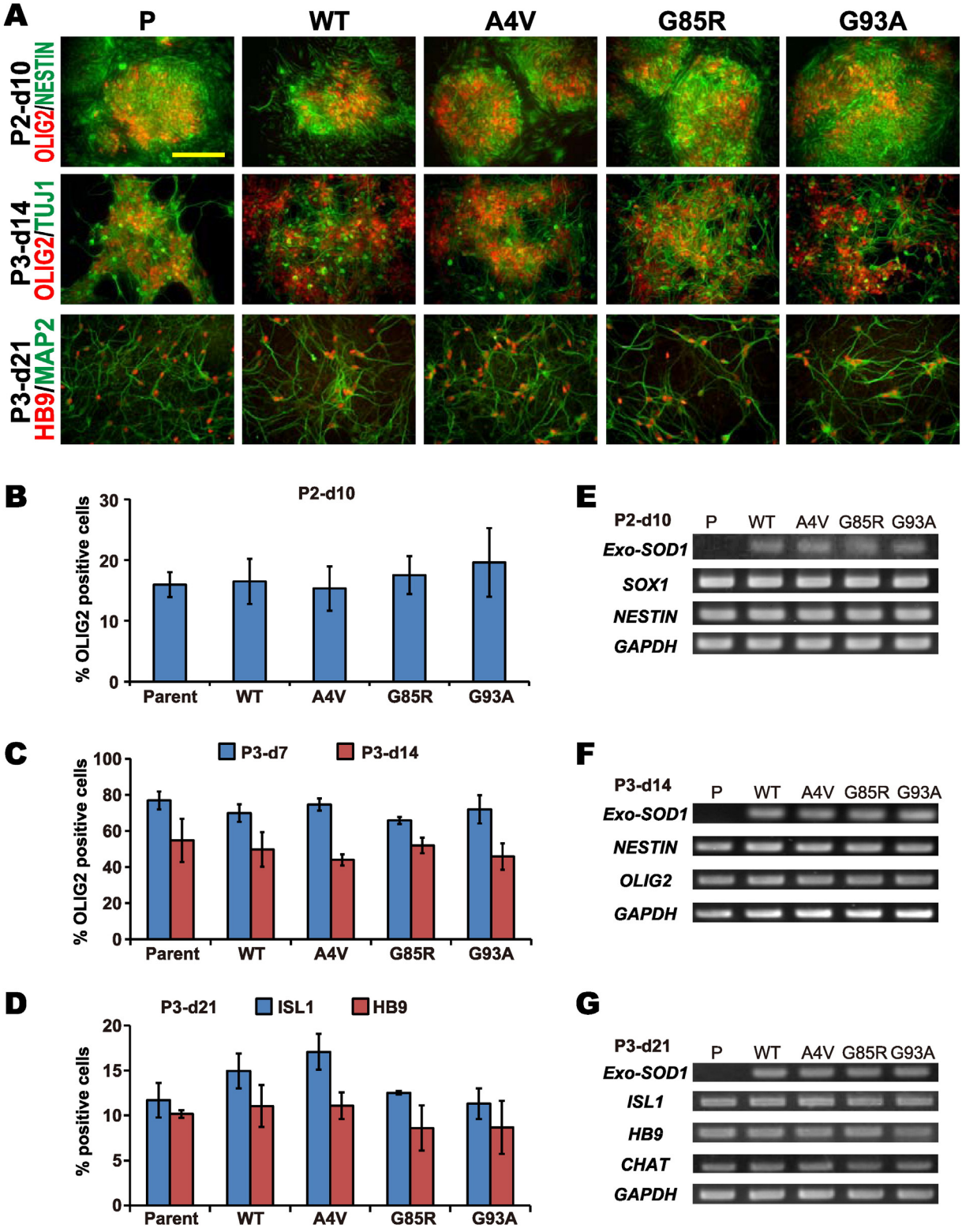

Fig. 3. Motor neuron differentiation of SOD1-hESCs. (A) Immunocytochemistry of the following neural markers: OLIG2 (a MN progenitor marker; red), nestin (a neural stem cell marker; green), TUJ1 (a neuron marker; green), HB9 (a MN marker; red) and MAP2 (a neuron marker; green) during MN differentiation. Cells on d10 in P2 (P2-d10), d14 in P3 (P3-d14), and d21 in P4 (P4-d21) were stained using neural marker antibodies. Scale bar, 100 μm. (B, C, D) Quantitative analysis of neural-marker-positive cells during MN differentiation. OLIG2-positive cells (B and C). ISL1-positive and HB9-positive cells (D). Values represent means ± SD (n = 3). (E, F, G) RT-PCR analysis using neurons on P2-d10 (E), P3-d14 (F), and P4-d21 (G). GAPDH was used as a loading control. (For interpretation of the references to color in this figure legend, the reader is referred to the web version of this article.)

including drugs tested in clinical ALS trials (Glicksman, 2011) (Limpert et al., 2013) (Lanka and Cudkowicz, 2008). We compared morphometric parameters of SOD1-MNs treated with chemicals or dimethyl sulfoxide (DMSO) as a control. Of these compounds, riluzole is the approved drug for ALS, and acts as a neuroprotective agent (Bellingham, 2011; Bensimon et al., 1994). After a 4-day treatment with 0.1 μM riluzole, only cells expressing G93A-SOD1 showed an extension of neurite length in ISL1, MAP2 double-positive MNs, while cells

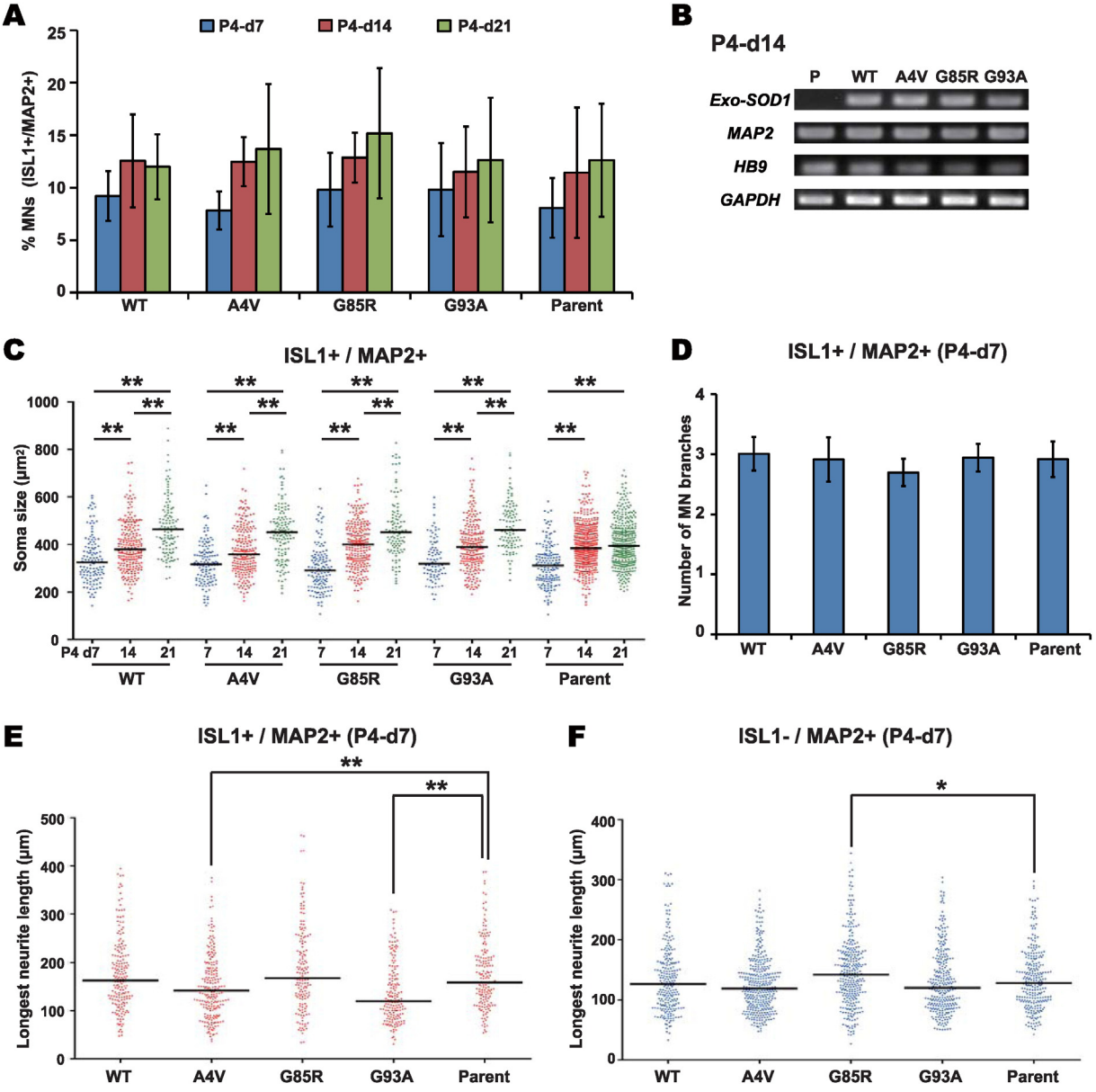

Fig. 4. Morphological changes in MNs derived from SOD1-hESCs. (A) The ratio of ISL1, MAP2-double positive MNs to MAP2 positive neurons during differentiation (P4-d7, blue; P4-d14, red; P4-d21, green). Values represent means ± SD (n = 4 to 7). (B) RT-PCR analysis of MNs on d14 in P4. GAPDH was used as a loading control. (C) Soma size (in μm^2) during MN differentiation (P4-d7, blue; P4-d14, red; P4-d21, green). The following sample sizes (n = 3 each) were counted in total: 82 to 155 neurons on P4-d7, 213 to 467 on P4-d14, and 99 to 357 on P4-d21. Black bars represent the median value. **P < 0.01, as determined by the Kruskal–Wallis test followed by Dunn's multiple comparison test. (D) The number of MN branches on d7 in P4. Values represent means ± SD (n = 10), P values were determined by the Kruskal–Wallis test followed by Dunn's multiple comparison test. (E) The longest neurite length (μm) of ISL1, MAP2 double-positive MNs on d7 in P4. Black bars represent the median value. The sample size was n = 3, with 153 to 185 neurons per sample counted in total. **P < 0.01, as determined by the Kruskal–Wallis test followed by Dunn's multiple comparison test. (F) The longest neurite length (in μm) of ISL1-negative and MAP2-positive cells on d7 in P4. Black bars represent the median value. The sample size was n = 3, with 237 to 342 neurons per sample counted in total. *P < 0.05, **P < 0.01, as determined by the Kruskal–Wallis test followed by Dunn's multiple comparison test. (For interpretation of the references to color in this figure legend, the reader is referred to the web version of this article.)

expressing WT-, A4V- and G93A-SOD1 showed similar effects in non-MNs (Fig. 5A, Supplementary Table S1). Changes in soma size were observed in MNs expressing A4V and G85R; however, there were no significant differences in the number of branches among any of the cell lines (Supplementary Fig. S4A and S4B, Supplementary Table S1).

Next, we examined the cellular responses to the drugs that resulted in neurite stabilization. The cyclic adenosine monophosphate (cAMP) signaling pathway plays a primary role in neurite stabilization (Hannila and Filbin, 2008). To activate this pathway, the cell-permeable cAMP analog dibutyryl-cAMP (dbcAMP) was used. In our cellular models, treatment with 1 mM dbcAMP increased neurite length in non-MNs derived from all cell lines (Fig. 5B). However, elongation of neurite length in MNs was only observed in cells expressing A4V and G93A (Fig. 5B, Supplementary Table S1). The soma sizes were expanded by dbcAMP treatment in MNs from both parental cell lines and those expressing G93A; the numbers of MN branches did not change in any of the cell lines (Supplementary Fig. S4C and S4D, Supplementary Table S1).

To determine the effect of compounds that induce neurite outgrowth in our ALS models, we used the Rho-associated protein kinase (ROCK) inhibitor, Y27632 (Dergham et al., 2002) (Fournier et al., 2003). ROCK acts as a mediator in growth inhibitory signaling that modulates growth cone stability by regulating actin dynamics (Uehata et al., 1997) (Tonges et al., 2011). In our cellular models, treatment with 10 μM Y27632 enhanced the neurite elongation of non-MNs in all cell lines; however, among MNs, this effect was confined to lines expressing A4V and G93A (Fig. 5C, Supplementary Table S1). Expansion in soma

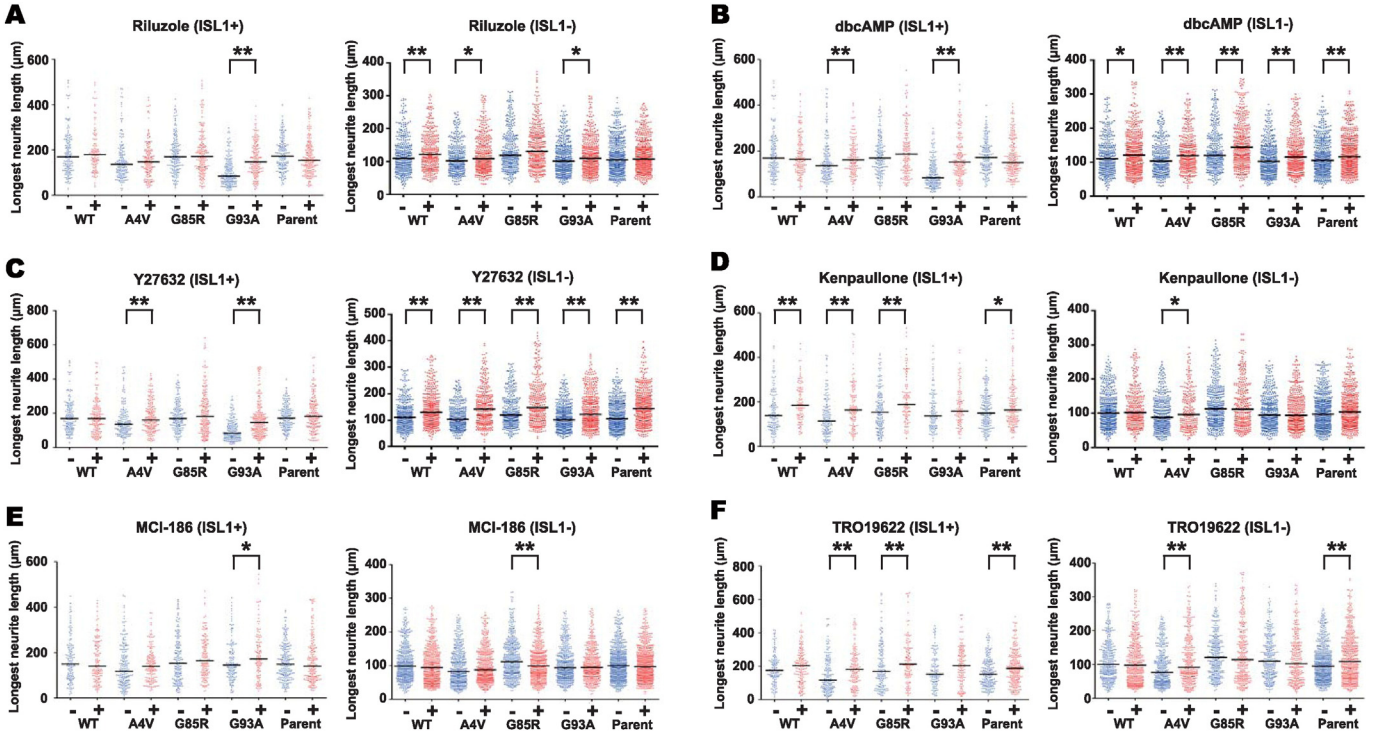

Fig. 5. Drug responses in MNs derived from SOD1-hESCs. Drug treatments were carried out from d3 to d7 in stage P4 cells. Measurement of the longest neurite length of ISL1, MAP2 double-positive (ISL1 +), or ISL1-negative, MAP2-positive neurons (ISL1-) on d7 in P4 was determined for cells receiving the following treatments (n = 3 each): (A) riluzole (0.1 μM), (B) dbcAMP (1 mM), (C) Y27632 (10 μM), (D) kenpaullone (5 μM), (E) MCI-186 (10 μM), and (F) TRO19622 (1 μM). *P < 0.05, **P < 0.01, as determined by the Mann–Whitney U test. Treatment with dimethyl sulfoxide (DMSO) as a control, −; treatment with compounds, +. The experiments using riluzole (A), dbcAMP (B) and Y27632 (C) were carried out simultaneously; therefore comparisons among the control data using DMSO were the same for these experiments.

size was observed only in MNs expressing G93A; there were no changes in the numbers of branches in MNs following Y27632 treatment (Supplementary Fig. S4E and S4F, Supplementary Table S1). These data suggest that although both dbcAMP and Y27632 are effective at inducing neurite elongation in non-MNs derived from all SOD1-hESCs, they only have this effect on MNs expressing A4V and G93A.

Recently, kenpaullone was identified as a potential drug candidate for the treatment of ALS disease using MNs derived from mouse ESCs expressing G93A-SOD1 (Yang et al., 2013). This compound is effective not only at promoting the in vitro survival of MNs expressing G93A-SOD1, but also that of MNs with other SOD1 mutations, including TDP43. In our cellular models, we found that the neurite length of MNs from the parental, WT, A4V, and G85R cell lines was increased following treatment with 5 μM kenpaullone although G93A did not (P = 0.06) (Fig. 5D, Supplementary Table S1). In the case of non-MNs, neurite length was only increased in cell lines expressing A4V (Fig. 5D). In all cell lines, the MN soma sizes were expanded, but there were no changes in the number of branches following treatment with kenpaullone (Supplementary Fig. S4G and S4H, Supplementary Table S1). These data indicate that kenpaullone was efficacious in altering ALS phenotypes in MNs, which is consistent with Yang's results (Yang et al., 2013).

Next, we tested MCI-186 and TRO19622, which have recently been listed in clinical trials as drug candidates for the treatment of ALS (Glicksman, 2011) (Limpert et al., 2013) (Lanka and Cudkowicz, 2008). MCI-186, also known as edaravone, is used for cerebral ischemia. It was found to be effective in a mouse ALS model with the G93A-SOD1 mutation (Ito et al., 2008). Recently, edaravone was approved as an ALS drug in Japan (www.mt-pharma.co.jp/e/release/nr/2015/pdf/e_MTPC150626_2.pdf). In our experiments, the administration of 10 μM MCI-186 promoted neurite elongation in MNs from cell lines expressing G93A alone, while shortening those in non-MNs expressing G85R (Fig. 5E, Supplementary Table S1). There were no effects on soma size or the number of branches in any of the cell lines (Supplementary Fig. S4I and S4J). These data suggest that effects of MCI-186 might be limited to specific mutations in SOD1 including G93A. Next, we tested the compound TRO19622, which failed in clinical trials (Lenglet et al., 2014). TRO19622 was first identified by a chemical screening assay utilizing rat primary MNs (Bordet et al., 2007) and promoted neurite outgrowth and survival in rat MNs in vitro (Bordet et al., 2007). Experiments in vivo showed that this compound improved motor performance, delayed the onset of the disease, and extended the life span of G93A-SOD1 transgenic mice (Bordet et al., 2007). In our model cells, the neurite length of MNs was promoted in the parental, A4V, and G85R cell lines following 1 μM TRO19622 treatment (Fig. 5F, Supplementary Table S1). Administration of TRO19622 did not increase the neurite length in MNs expressing G93A (P = 0.068), but enhanced neurite length in non-MNs from A4V and parental cell lines. Soma size decreased in MNs from both in WT and parental cell lines, while the branch numbers decreased in MNs from the parental and G93A cell lines (Supplementary Fig. S4K and S4L, Supplementary Table S1). These data suggest that TRO19622 may also be effective at treating ALS phenotypes in MNs with specific SOD1 mutations.

Furthermore, in order to investigate drug responses, we performed dose–response assays using riluzole and MCI-186. Riluzole at a concentration of 100 nM was effective in G93A-MNs, while a lower concentration (10 nM alone) was efficacious in A4V-MNs to enhance neurite length (Fig. 6A). Higher concentrations of riluzole did not affect neurite length of MNs in our ALS models. These results suggest that the effective concentration of riluzole might be dependent on SOD1 mutation types. On the other hand, MCI-186 enhanced the neurite length in G93A-MNs at both 10 and 100 μM (Fig. 6B). This compound was not effective in the parent and other mutation types of SOD1-MNs at the concentrations examined. Collectively, the results of the dose–response assays indicated that ALS models expressing different SOD1 mutations displayed differential responses to ALS drugs.

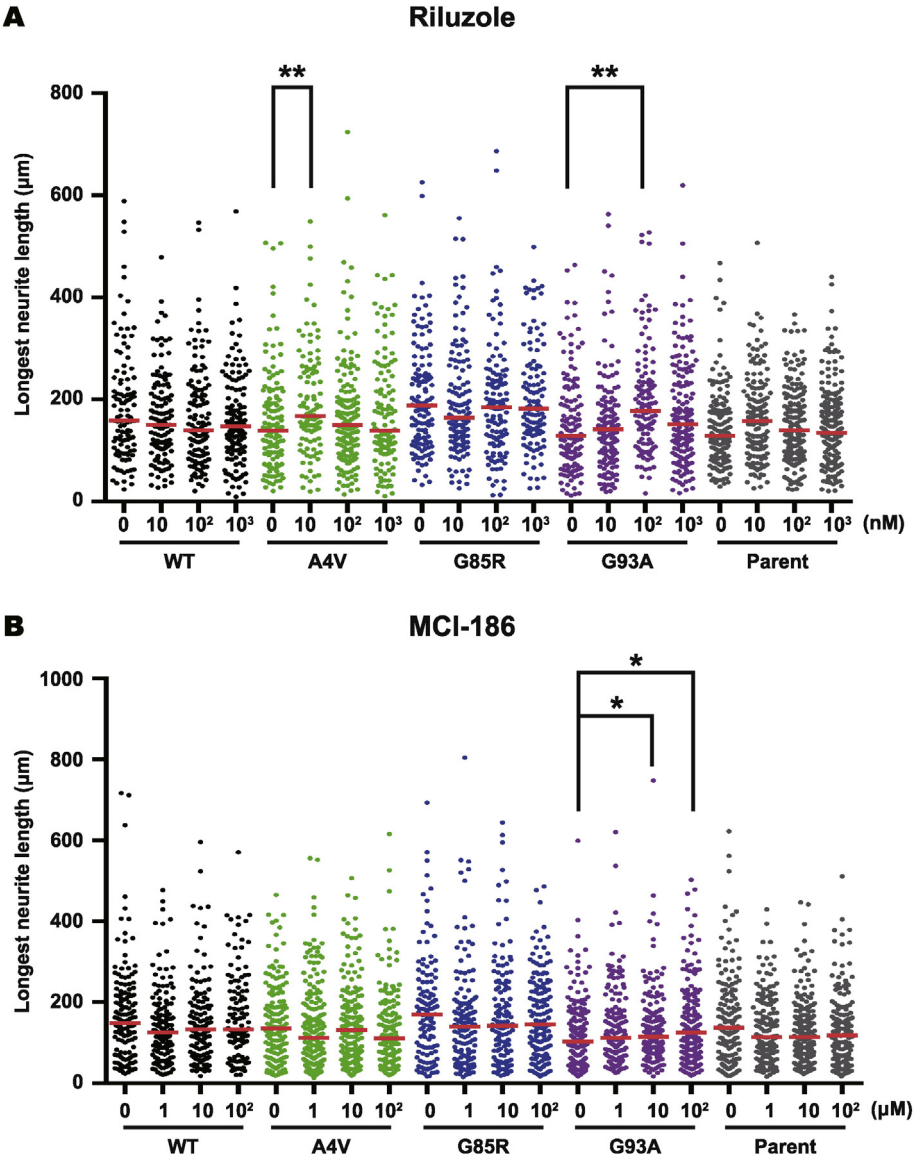

Fig. 6. Dose–response of ALS drugs in MNs derived from SOD1-hESCs. Drug treatments were carried out from d3 to d7 in stage P4 cells. Measurement of the longest neurite length of ISL1, MAP2 double-positive MNs was done. DMSO was used as a control without drug treatment. (A) The concentrations of riluzole were 10, 100 and 1000 nM (n = 4). (B) The concentrations of MCI-186 were 1, 10 and100 μM (n = 3). *P < 0.05, **P < 0.01, as determined by the Steel's test. Red bars represent the median value. (For interpretation of the references to color in this figure legend, the reader is referred to the web version of this article.)

4. Discussion

It is known that mutation types of SOD1 affect not only enzymatic activity and protein half-life of SOD1, but also age at onset and the survival time of SOD1-ALS patients (Hayward et al., 2002) (Borchelt et al., 1994) (Regal et al., 2006). However, there are very few studies focusing on comparative study of SOD1 mutations. Here, we generated SOD1-ALS models derived from mutant SOD1-overexpressing hESCs with identical genetic background and we found mutation-specific morphological alterations. Furthermore, our models revealed that mutation types affect drug responses.

Recently, two papers reported that mutant SOD1s influenced not only cell death but also the morphologies such as soma size, neurite length and abnormal organelles in MNs derived from the patient-specific iPSCs (Chen et al., 2014; Kiskinis et al., 2014). Although cell death was not detected in our ALS models, the reduction of neurite length, which could be a cellular disease phenotype, was observed in our ALS models except in G85R-SOD1. Morphological changes, primarily the elongation of MN neurite length, were detected following treatment with the compounds we investigated. Atrophic changes or axonopathy of MNs is observed in ALS (Ferraiuolo et al., 2011; Fischer et al., 2004; Vinsant et al., 2013); hence, the MN neurite length change of our ALS models might be a good predictor of drug efficacy in ALS. Our ALS models have potential as cell materials for cell-based high-throughput drug screening, similar to previous studies using patient-iPSCs (Egawa et al., 2012) (Yang et al., 2013).

Interestingly, the cellular phenotype could also be classified by differences in SOD1-mutation-dependent responses to the same compound. Since our models have an identical genetic background, these differential responses were caused by differences in SOD1 mutations. Therefore, our ALS models are promising tools for investigating the role and toxicity of mutant SOD1 on disease onset and progression as well as differential drug responses.

Results from this study suggest that mutant-specific experimental and clinical strategies may be required for drug discovery and clinical trials. However, it is unclear how much individual genetic background affects mutant-specific strategies. In addition, gene overexpression approach has limitations such as unnatural gene expression and limited

applicability. In fact, we haven't established any mutant TDP43-expresssing hESC lines by our gene integration system (data not shown). Future research on drug response-based classification using SOD1-ALS patient-derived iPSCs with different genetic background might be interesting and worthwhile.

Riluzole, which is widely used and the approved drug for ALS, showed effects on A4V- and G93A-MNs at a single concentration of 10 and 100 nM, respectively, in our models. It is unclear why the drug was effective at a single dose but not in a dose-dependent manner in this study. This drug was reported to provide protective effects to primary rat MNs treated with media conditioned from primary astrocytes derived from mouse ALS models (including G93A and G86R SOD1 variants) (Rojas et al., 2014). Similarly, MCI-186, which is known as a neuroprotective drug (Shichinohe et al., 2004), only affected the elongation of neurites in MNs expressing G93A-SOD1. These results suggest that neuroprotective drugs might be effective at treating ALS phenotypes with respect to non-cell-autonomous toxicity or specific types of SOD1 mutations.

Mutant SOD1 variants are divided into two classes on the basis of the metal ion content and the position of the mutation: WT-like mutants and metal-binding region (MBR) mutants (Rodriguez et al., 2002; Tiwari and Hayward, 2005). A4V and G93A are WT-like mutants, whereas G85R is a MBR mutant. We found that dbcAMP and Y27632 showed efficacy in non-MNs from all mutant-SOD1, WT-SOD1, and parental cell lines examined. However, they were only effective in MNs from cell lines expressing SOD1 variants in the WT-like mutant group. In contrast, kenpaullone was not effective at increasing the longest neurite length in non-MNs, but was widely effective in MNs, regardless of mutation type (although the effects on MNs expressing G93A were not statistically significant). TRO19622 showed effectiveness similar to kenpaullone despite the fact that the targets of these two compounds are different: TRO19622 inhibits the mitochondrial permeability transition pore complex (Bordet et al., 2007), while kenpaullone inhibits glycogen synthase kinase 3 and some cyclin-dependent kinases (Martinez et al., 2002; Senderowicz and Sausville, 2000).

In this study, out of over 100 SOD1 mutants, only three SOD1 mutants were examined. By using SOD1-ALS models with a large number of other mutation types, SOD1 mutations could be potentially classified into drug response-based categories. Astrocytes are additionally implicated in MN death by secretion of neurotoxic factors (Wada et al., 2012) (Yamanaka et al., 2008) (Re et al., 2014) (Rojas et al., 2014) (Nagai et al., 2007). To the best of our knowledge, there are no reports that astrocytes show SOD1 mutation-dependent responses to drug in a manner similar to MNs. Future research should address questions regarding the classification of ALS into treatment-responsive categories and the associated role of astrocytes.

Author contributions

TI, NN, and KA conceived and designed the experiments. TI and NT performed the experiments. TI analyzed the data, and TI and KA wrote the paper.

Competing financial interests

NN is a shareholder of ReproCELL. TI, NT, and KA declare no potential conflict of interest.

Acknowledgments

We thank Dr. Sravan K. Goparaju for critical reading our manuscript. This work was supported in part by JSPS KAKENHI (23500446) and the iCeMS exploratory grant for junior investigators to KA. TI was supported in part by the Global COE Program “Center for Frontier Medicine”, MEXT, Japan (F09) as a predoctoral fellow. The iCeMS is supported by World Premier International Research Center Initiative (WPI).

Appendix A Supplementary data

Supplementary data to this article can be found online at http://dx.doi.org/10.1016/j.scr.2015.09.006.

References

Beckman, J.S., Estevez, A.G., Crow, J.P., Barbeito, L., 2001. Superoxide dismutase and the death of motoneurons in ALS. Trends Neurosci. 24, S15–S20.
Bellingham, M.C., 2011. A review of the neural mechanisms of action and clinical efficiency of riluzole in treating amyotrophic lateral sclerosis: what have we learned in the last decade? CNS Neurosci. Ther. 17, 4–31.
Bensimon, G., Lacomblez, L., Meininger, V., 1994. A controlled trial of riluzole in amyotrophic lateral sclerosis. ALS/Riluzole Study Group. N. Engl. J. Med. 330, 585–591.
Bilican, B., Serio, A., Barmada, S.J., Nishimura, A.L., Sullivan, G.J., Carrasco, M., Phatnani, H.P., Puddifoot, C.A., Story, D., Fletcher, J., et al., 2012. Mutant induced pluripotent stem cell lines recapitulate aspects of TDP-43 proteinopathies and reveal cell-specific vulnerability. Proc. Natl. Acad. Sci. U. S. A. 109, 5803–5808.
Borchelt, D.R., Lee, M.K., Slunt, H.S., Guarnieri, M., Xu, Z.S., Wong, P.C., Brown Jr., R.H., Price, D.L., Sisodia, S.S., Cleveland, D.W., 1994. Superoxide dismutase 1 with mutations linked to familial amyotrophic lateral sclerosis possesses significant activity. Proc. Natl. Acad. Sci. U. S. A. 91, 8292–8296.
Bordet, T., Buisson, B., Michaud, M., Drouot, C., Galea, P., Delaage, P., Akentieva, N.P., Evers, A.S., Covey, D.F., Ostuni, M.A., et al., 2007. Identification and characterization of cholest-4-en-3-one, oxime (TRO19622), a novel drug candidate for amyotrophic lateral sclerosis. J. Pharmacol. Exp. Ther. 322, 709–720.
Bruijn, L.I., Miller, T.M., Cleveland, D.W., 2004. Unraveling the mechanisms involved in motor neuron degeneration in ALS. Annu. Rev. Neurosci. 27, 723–749.
Bryan, B.A., Cai, Y., Liu, M., 2006. The Rho-family guanine nucleotide exchange factor GEFT enhances retinoic acid- and cAMP-induced neurite outgrowth. J. Neurosci. Res. 83, 1151–1159.
Chen, H., Qian, K., Du, Z., Cao, J., Petersen, A., Liu, H., Blackbourn, L.W.t., Huang, C.L., Errigo, A., Yin, Y., et al., 2014. Modeling ALS with iPSCs reveals that mutant SOD1 misregulates neurofilament balance in motor neurons. Cell Stem Cell 14, 796–809.
Dergham, P., Ellezam, B., Essagian, C., Avedissian, H., Lubell, W.D., McKerracher, L., 2002. Rho signaling pathway targeted to promote spinal cord repair. J. Neurosci. 22, 6570–6577.
Egawa, N., Kitaoka, S., Tsukita, K., Naitoh, M., Takahashi, K., Yamamoto, T., Adachi, F., Kondo, T., Okita, K., Asaka, I., et al., 2012. Drug screening for ALS using patient-specific induced pluripotent stem cells. Science Translational Medicine. 4, p. 145ra104.
Ferraiuolo, L., Kirby, J., Grierson, A.J., Sendtner, M., Shaw, P.J., 2011. Molecular pathways of motor neuron injury in amyotrophic lateral sclerosis. Nat. Rev. Neurol. 7, 616–630.
Fischer, L.R., Culver, D.G., Tennant, P., Davis, A.A., Wang, M., Castellano-Sanchez, A., Khan, J., Polak, M.A., Glass, J.D., 2004. Amyotrophic lateral sclerosis is a distal axonopathy: evidence in mice and man. Exp. Neurol. 185, 232–240.
Fournier, A.E., Takizawa, B.T., Strittmatter, S.M., 2003. Rho kinase inhibition enhances axonal regeneration in the injured CNS. J. Neurosci. 23, 1416–1423.
Glicksman, M.A., 2011. The preclinical discovery of amyotrophic lateral sclerosis drugs. Expert Opin.Drug Discovery 6, 1127–1138.
Gunther, R., Saal, K.A., Suhr, M., Scheer, D., Koch, J.C., Bahr, M., Lingor, P., Tonges, L., 2014. The rho kinase inhibitor Y-27632 improves motor performance in male SOD1(G93A) mice. Front. Neurosci. 8, 304.
Hannila, S.S., Filbin, M.T., 2008. The role of cyclic AMP signaling in promoting axonal regeneration after spinal cord injury. Exp. Neurol. 209, 321–332.
Hayward, L.J., Rodriguez, J.A., Kim, J.W., Tiwari, A., Goto, J.J., Cabelli, D.E., Valentine, J.S., Brown Jr., R.H., 2002. Decreased metallation and activity in subsets of mutant superoxide dismutases associated with familial amyotrophic lateral sclerosis. J. Biol. Chem. 277, 15923–15931.
Ito, H., Wate, R., Zhang, J., Ohnishi, S., Kaneko, S., Nakano, S., Kusaka, H., 2008. Treatment with edaravone, initiated at symptom onset, slows motor decline and decreases SOD1 deposition in ALS mice. Exp. Neurol. 213, 448–455.
Kiskinis, E., Sandoe, J., Williams, L.A., Boulting, G.L., Moccia, R., Wainger, B.J., Han, S., Peng, T., Thams, S., Mikkilineni, S., et al., 2014. Pathways disrupted in human ALS motor neurons identified through genetic correction of mutant SOD1. Cell Stem Cell 14, 781–795.
Lanka, V., Cudkowicz, M., 2008. Therapy development for ALS: lessons learned and path forward. Amyotroph. Lateral Scler.: Official Publication of the World Federation of Neurology Research Group on Motor Neuron Diseases 9, 131–140.
Lenglet, T., Lacomblez, L., Abitbol, J.L., Ludolph, A., Mora, J.S., Robberecht, W., Shaw, P.J., Pruss, R.M., Cuvier, V., Meininger, V., 2014. A phase II–III trial of olesoxime in subjects with amyotrophic lateral sclerosis. Eur. J. Neurol.: The Official Journal of the European Federation of Neurological Societies 21, 529–536.
Limpert, A.S., Mattmann, M.E., Cosford, N.D., 2013. Recent progress in the discovery of small molecules for the treatment of amyotrophic lateral sclerosis (ALS). Beilstein J. Org. Chem. 9, 717–732.
Lyall, R.A., Donaldson, N., Polkey, M.I., Leigh, P.N., Moxham, J., 2001. Respiratory muscle strength and ventilatory failure in amyotrophic lateral sclerosis. Brain: a journal of neurology 124, 2000–2013.

Martinez, A., Castro, A., Dorronsoro, I., Alonso, M., 2002. Glycogen synthase kinase 3 (GSK-3) inhibitors as new promising drugs for diabetes, neurodegeneration, cancer, and inflammation. Med. Res. Rev. 22, 373–384.

Millecamps, S., Salachas, F., Cazeneuve, C., Gordon, P., Bricka, B., Camuzat, A., Guillot-Noel, L., Russaouen, O., Bruneteau, G., Pradat, P.F., et al., 2010. SOD1, ANG, VAPB, TARDBP, and FUS mutations in familial amyotrophic lateral sclerosis: genotype-phenotype correlations. J. Med. Genet. 47, 554–560.

Nagai, M., Re, D.B., Nagata, T., Chalazonitis, A., Jessell, T.M., Wichterle, H., Przedborski, S., 2007. Astrocytes expressing ALS-linked mutated SOD1 release factors selectively toxic to motor neurons. Nat. Neurosci. 10, 615–622.

Neumann, M., Sampathu, D.M., Kwong, L.K., Truax, A.C., Micsenyi, M.C., Chou, T.T., Bruce, J., Schuck, T., Grossman, M., Clark, C.M., et al., 2006. Ubiquitinated TDP-43 in frontotemporal lobar degeneration and amyotrophic lateral sclerosis. Science 314, 130–133.

Re, D.B., Le Verche, V., Yu, C., Amoroso, M.W., Politi, K.A., Phani, S., Ikiz, B., Hoffmann, L., Koolen, M., Nagata, T., et al., 2014. Necroptosis drives motor neuron death in models of both sporadic and familial ALS. Neuron 81, 1001–1008.

Regal, L., Vanopdenbosch, L., Tilkin, P., Van den Bosch, L., Thijs, V., Sciot, R., Robberecht, W., 2006. The G93C mutation in superoxide dismutase 1: clinicopathologic phenotype and prognosis. Arch. Neurol. 63, 262–267.

Renton, A.E., Chio, A., Traynor, B.J., 2014. State of play in amyotrophic lateral sclerosis genetics. Nat. Neurosci. 17, 17–23.

Renton, A.E., Majounie, E., Waite, A., Simon-Sanchez, J., Rollinson, S., Gibbs, J.R., Schymick, J.C., Laaksovirta, H., van Swieten, J.C., Myllykangas, L., et al., 2011. A hexanucleotide repeat expansion in C9ORF72 is the cause of chromosome 9p21-linked ALS-FTD. Neuron 72, 257–268.

Rodriguez, J.A., Valentine, J.S., Eggers, D.K., Roe, J.A., Tiwari, A., Brown Jr., R.H., Hayward, L.J., 2002. Familial amyotrophic lateral sclerosis-associated mutations decrease the thermal stability of distinctly metallated species of human copper/zinc superoxide dismutase. J. Biol. Chem. 277, 15932–15937.

Rojas, F., Cortes, N., Abarzua, S., Dyrda, A., van Zundert, B., 2014. Astrocytes expressing mutant SOD1 and TDP43 trigger motoneuron death that is mediated via sodium channels and nitroxidative stress. Front. Cell. Neurosci. 8, 24.

Rosen, D.R., Siddique, T., Patterson, D., Figlewicz, D.A., Sapp, P., Hentati, A., Donaldson, D., Goto, J., O'Regan, J.P., Deng, H.X., et al., 1993. Mutations in Cu/Zn superoxide dismutase gene are associated with familial amyotrophic lateral sclerosis. Nature 362, 59–62.

Sakurai, K., Shimoji, M., Tahimic, C.G., Aiba, K., Kawase, E., Hasegawa, K., Amagai, Y., Suemori, H., Nakatsuji, N., 2010. Efficient integration of transgenes into a defined locus in human embryonic stem cells. Nucleic Acids Res. 38, e96.

Senderowicz, A.M., Sausville, E.A., 2000. Preclinical and clinical development of cyclin-dependent kinase modulators. J. Natl. Cancer Inst. 92, 376–387.

Shichinohe, H., Kuroda, S., Yasuda, H., Ishikawa, T., Iwai, M., Horiuchi, M., Iwasaki, Y., 2004. Neuroprotective effects of the free radical scavenger Edaravone (MCI-186) in mice permanent focal brain ischemia. Brain Res. 1029, 200–206.

Suemori, H., Yasuchika, K., Hasegawa, K., Fujioka, T., Tsuneyoshi, N., Nakatsuji, N., 2006. Efficient establishment of human embryonic stem cell lines and long-term maintenance with stable karyotype by enzymatic bulk passage. Biochem. Biophys. Res. Commun. 345, 926–932.

Tiwari, A., Hayward, L.J., 2005. Mutant SOD1 instability: implications for toxicity in amyotrophic lateral sclerosis. Neurodegener. Dis. 2, 115–127.

Tonges, L., Koch, J.C., Bahr, M., Lingor, P., 2011. ROCKing regeneration: rho kinase inhibition as molecular target for neurorestoration. Front. Mol. Neurosci. 4, 39.

Uehata, M., Ishizaki, T., Satoh, H., Ono, T., Kawahara, T., Morishita, T., Tamakawa, H., Yamagami, K., Inui, J., Maekawa, M., et al., 1997. Calcium sensitization of smooth muscle mediated by a rho-associated protein kinase in hypertension. Nature 389, 990–994.

Vance, C., Rogelj, B., Hortobagyi, T., De Vos, K.J., Nishimura, A.L., Sreedharan, J., Hu, X., Smith, B., Ruddy, D., Wright, P., et al., 2009. Mutations in FUS, an RNA processing protein, cause familial amyotrophic lateral sclerosis type 6. Science 323, 1208–1211.

Vinsant, S., Mansfield, C., Jimenez-Moreno, R., Del Gaizo Moore, V., Yoshikawa, M., Hampton, T.G., Prevette, D., Caress, J., Oppenheim, R.W., Milligan, C., 2013. Characterization of early pathogenesis in the SOD1(G93A) mouse model of ALS: part I, background and methods. Brain Behav. 3, 335–350.

Wada, T., Goparaju, S.K., Tooi, N., Inoue, H., Takahashi, R., Nakatsuji, N., Aiba, K., 2012. Amyotrophic lateral sclerosis model derived from human embryonic stem cells overexpressing mutant superoxide dismutase 1. Stem cells Transl. Med. 1, 396–402.

Wada, T., Honda, M., Minami, I., Tooi, N., Amagai, Y., Nakatsuji, N., Aiba, K., 2009. Highly efficient differentiation and enrichment of spinal motor neurons derived from human and monkey embryonic stem cells. PLoS One 4, e6722.

Wang, L., Deng, H.X., Grisotti, G., Zhai, H., Siddique, T., Roos, R.P., 2009. Wild-type SOD1 overexpression accelerates disease onset of a G85R SOD1 mouse. Hum. Mol. Genet. 18, 1642–1651.

Yamanaka, K., Chun, S.J., Boillee, S., Fujimori-Tonou, N., Yamashita, H., Gutmann, D.H., Takahashi, R., Misawa, H., Cleveland, D.W., 2008. Astrocytes as determinants of disease progression in inherited amyotrophic lateral sclerosis. Nat. Neurosci. 11, 251–253.

Yang, Y.M., Gupta, S.K., Kim, K.J., Powers, B.E., Cerqueira, A., Wainger, B.J., Ngo, H.D., Rosowski, K.A., Schein, P.A., Ackeifi, C.A., et al., 2013. A small molecule screen in stem-cell-derived motor neurons identifies a kinase inhibitor as a candidate therapeutic for ALS. Cell Stem Cell 12, 713–726.